RADIATION RESEARCH **188**, 191–203 (2017)
0033-7587/17 $15.00

DOI: 10.1667/RR14667.1

Different Sequences of Fractionated Low-Dose Proton and Single Iron-Radiation-Induced Divergent Biological Responses in the Heart

Sharath P. Sasi,[a] Xinhua Yan,[a,b] Marian Zuriaga-Herrero,[f] Hannah Gee,[a] Juyong Lee,[c] Raman Mehrzad,[d] Jin Song,[a] Jillian Onufrak,[a] James Morgan,[b,d] Heiko Enderling,[e] Kenneth Walsh,[f] Raj Kishore[g] and David A. Goukassian[a,f,g,1]

[a] *Cardiovascular Research Center, GeneSys Research Institute, Boston, Massachusetts;* [b] *Tufts University School of Medicine, Boston, Massachusetts;* [c] *Calhoun Cardiology Center, University of Connecticut Health Center, Farmington, Connecticut;* [d] *Steward Carney Hospital, Dorchester, Massachusetts;* [e] *Department of Integrated Mathematical Oncology, H. Lee Moffitt Cancer Center and Research Institute, Tampa, Florida;* [f] *Whitaker Cardiovascular Institute, Boston University School of Medicine, Boston, Massachusetts; and* [7] *Center for Translational Medicine, Temple University School of Medicine, Philadelphia, Pennsylvania*

Sasi, S. P., Yan, X., Zuriaga-Herrero, M., Gee, H., Lee, J., Mehrzad, R., Song, J., Onufrak, J., Morgan, J., Enderling, H., Walsh, K., Kishore, R. and Goukassian, D. A. Different Sequences of Fractionated Low-Dose Proton and Single Iron-Radiation-Induced Divergent Biological Responses in the Heart. ***Radiat. Res.*** **188, 191–203 (2017).**

Deep-space travel presents risks of exposure to ionizing radiation composed of a spectrum of low-fluence protons (^{1}H) and high-charge and energy (HZE) iron nuclei (e.g., ^{56}Fe). When exposed to galactic cosmic rays, each cell in the body may be traversed by ^{1}H every 3–4 days and HZE nuclei every 3–4 months. The effects of low-dose sequential fractionated ^{1}H or HZE on the heart are unknown. In this animal model of simulated ionizing radiation, middle-aged (8–9 months old) male C57BL/6NT mice were exposed to radiation as follows: group 1, nonirradiated controls; group 2, three fractionated doses of 17 cGy ^{1}H every other day ($^{1}H \times 3$); group 3, three fractionated doses of 17 cGy ^{1}H every other day followed by a single low dose of 15 cGy ^{56}Fe two days after the final ^{1}H dose ($^{1}H \times 3 + {}^{56}Fe$); and group 4, a single low dose of 15 cGy ^{56}Fe followed (after 2 days) by three fractionated doses of 17 cGy ^{1}H every other day ($^{56}Fe + {}^{1}H \times 3$). A subgroup of mice from each group underwent myocardial infarction (MI) surgery at 28 days postirradiation. Cardiac structure and function were assessed in all animals at days 7, 14 and 28 after MI surgery was performed. Compared to the control animals, the treatments that groups 2 and 3 received did not induce negative effects on cardiac function or structure. However, compared to all other groups, the animals in group 4, showed depressed left ventricular (LV) functions at 1 month with concomitant enhancement in cardiac fibrosis and induction of cardiac hypertrophy signaling at 3 months. In the irradiated and MI surgery groups compared to the control group, the treatments received by groups 2 and 4 did not induce negative effects at 1 month postirradiation and MI surgery. However, in group 3 after MI surgery, there was a 24% increase in mortality, significant decreases in LV function and a 35% increase in post-infarction size. These changes were associated with significant decreases in the angiogenic and cell survival signaling pathways. These data suggest that fractionated doses of radiation induces cellular and molecular changes that result in depressed heart functions both under basal conditions and particularly after myocardial infarction.

INTRODUCTION

Deep-space exploration-type manned missions to Mars that have been planned for early 2030 would involve exposure of astronauts to various stressors, including reduced gravity and different types of space radiation, for up to three years (*1, 2*). In contrast, the space radiation environment for current low-Earth orbit (LEO) missions is drastically different from deep space, primarily aided by the protection provided by the Earth's magnetic field and shielding within the spacecraft, which significantly attenuate pathological events (*3, 4*). The earth's surface encompasses low-linear energy transfer (LET) radiations primarily comprised of neutrons from cosmic radiation and alpha particles from terrestrial radionuclides (*4*). However, beyond LEO, the effects of radiation become more onerous, solely due to ionizing radiation arising from a broad range of high-LET particles (*2–4*), comprising a toxic milieu of galactic cosmic radiation (GCR) and particles expelled during solar particle events (SPEs) (*3, 5*). A significant amount of radiation in space is composed of GCR and consists of predominantly high-energy protons (~85% hydrogen ions, ^{1}H; $Z = 1$) along with alpha particles (~12% helium ions, ^{2}He; $Z = 2$), minimal-hazard electrons and positrons (~1%) and heavy ions of up to 10,000 GeV energies [also known as high-charge and energy (HZE) nuclei] that comprise only ~1% of particles (*2, 4, 6–9*). Along with GCR, unpredictable and intermittent SPEs can produce large plasma clouds essentially comprised of low-LET protons (up to 1 GeV/nucleon energy) (*4, 5, 7*)

[1] Address for correspondence: Center for Translational Medicine, Temple University School of Medicine, 3500 N. Broad Street, MERB 972B, Philadelphia, PA 19140; email: david.goukassian@temple.edu.

sometimes mixed with high-density fluxes of protons with energies mounting to >30 MeV (*10*). Furthermore, interaction of these HZE and SPE particles with shielding material on the spacecraft and biological material can result in secondary ionizing radiation hazards such as gamma, electrons, neutrons, pions, muons, etc. (*3, 4*). It has been estimated that during deep-space missions, each cell in an astronaut's body will be traversed by a ^{1}H nucleus every few days, a ^{2}He nucleus every few weeks and HZE nuclei [e.g., carbon (^{12}C), oxygen (^{16}O), silicon (^{28}Si), iron (^{56}Fe), etc.] every few months (*11, 12*). HZE-induced radiation damage is substantial due to extremely high LET (*13, 14*) and the density of ionizing events deposited along the trajectory of the particles that can result in cluster DNA damage, often in the form of irreparable track damage to individual cells and tissue (*15*).

With extended stays beyond the Earth's protective magnetosphere during deep-space missions, there is substantial concern about the potential long-term risks to the astronauts and the acceptable risk levels associated with exposure to HZE ionizing particles or combined SPE and GCR. Due to practical and financial limitations associated with strategies for increasing shielding on the spacecraft, exposure to such fast-moving energetic particles is inevitable (*16*). One of the major concerns associated with accumulated exposure to ionizing space radiation beyond LEO is the distinct type of biological damage and response triggered by each type and dose of radiation in a cell or tissue environment (*3, 17, 18*). Reports have indicated that as much as 0.4–0.8 mGy/day tissue dose rates are delivered from GCR (*19*). Measurement on the Mars Science Laboratory's Curiosity Rover had estimated the total mission dose equivalent of ~1.01 Sv (equivalent to 1 Gy of X and gamma rays) for a round trip Mars surface mission, with 12 months in transit and 500 days on the Martian surface using the current solar cycle data (*20*). In addition, there may be a ~2 Gy proton-radiation dose to the whole body of the astronaut arising from a large SPE (*21–24*). Another space stressor, microgravity, when combined with ionizing space radiation, may accentuate degenerative tissue responses that can affect several organs, including heart and vasculature, for which there is currently no adequate risk information (*3, 9*).

Although extensive epidemiologic evidence has highlighted cardiovascular (CV) diseases as secondary morbidity and mortality risks due to radiation exposure in radiotherapy patients (*25–29*) and after unintended nonoccupational exposure (*30–32*), there is very limited information on the direct effects of space radiation on the CV system and long-term degenerative risks associated with exposure to mixed HZE particles or protons. The majority of space flight-associated CV risks identified to date were determined shortly after LEO missions and include cardiac dysrhythmias, compromised orthostatic CV response, manifestation of previously asymptomatic CV disease and cardiac atrophy (*1, 33, 34*). The lack of human epidemiology data for SPE-like proton and HZE-particle radiations along with multifactorial nature of CV diseases and their long latency periods makes risk predictions highly uncertain (*35*). Most high- and low-LET radiation based studies have shown detrimental effects on parameters such as angiogenesis (*36*), endothelial dysfunction (*37*) and endothelial cell damage (*9*) contributing to vascular and circulatory diseases (*38*). In light of these recent studies and reviews, a threshold dose of 0.5 Gy was proposed (*39*) particularly for degenerative risks manifesting very late after exposure with circulatory diseases to be of great importance for a mission to Mars (*2*).

Contingent upon these parameters, we previously reported the effects of a single, whole-body, low-dose ^{1}H (0.50 Gy, 1 GeV) and ^{56}Fe (0.15 Gy, 1 GeV/nucleon) ion irradiation on the CV system during normal aging and under ischemic conditions (*40*). These studies signified the long-term (up to 10 months) postirradiation negative effects on the myocardium, systolic and diastolic heart functions accompanied by increased hypertrophic signaling contributing to heart failure (*40*). A myocardial infarction (MI) after exposure to 0.15 Gy low-dose high-energy ^{56}Fe radiation demonstrated long-lasting detrimental effects including loss of cardiac function and worsened cardiac remodeling over the period of 10 months. On the other hand, 0.5 Gy ^{1}H irradiation induced positive effects during recovery after a MI event (*40*), which may be attributed to a possible ischemic preconditioning-like effect of low-proton irradiation of the heart (*41*).

Because there is essentially no data available on the effects of different sequential, fractionated low-dose charged particle (SPE-like proton and HZE) irradiations to the CV system, we used murine models to examine the effects of acute, whole-body fractionated low-dose ^{1}H exposure by itself and in combination with a single low dose of ^{56}Fe radiation to emulate a possible space-like environment. Our findings provide initial mechanistic insight into the development of CV morbidity and mortality induced by mixed charged particle radiation in the heart tissue.

MATERIALS AND METHODS

Animal Models

Adult male C57Bl/6NT mice, 8–10 months of age (Taconic, Germantown, NY) were used for the entire study. Animals were shipped directly to Brookhaven National Laboratory (BNL, Upton, NY) where they were fed standard laboratory chow diet (Harlan Teklad, Madison, WI), given water access *ad libitum* and kept in a temperature-controlled environment on a 12:12 h light-dark schedule. All mice were handled in accordance with the guidelines set and approved by the Institutional Animal Care and Use Committees (IACUC) at both GeneSys Research Institute (Boston, MA) and BNL. Any animal in this study found to exhibit severe or irreversible symptoms of pain and distress (limited mobility, reduced consumption of food and water, weight loss of 15% or more) was euthanized immediately by pentobarbital-based euthanasia solution 200 mg/kg intraperitoneal (i.p.) injection, which is consistent with the recom-

mendation of the Panel on Euthanasia of the American Veterinary Medical Association Guidelines on Euthanasia.

Particle Irradiation and Dosimetry

Whole-body exposures of mice to 1 GeV hydrogen protons (^{1}H; LET = 0.223 keV/μm) and 1 GeV/nucleon iron ions (^{56}Fe; LET = 151.4 keV/μm) were performed at the NASA Space Radiation Laboratory at BNL according to standardized procedures. Individual rectangular polystyrene boxes with multiple air holes (4 mm in diameter) were used to house animals during three fractionated sequential doses of ~17 cGy ^{1}H (total dose of 50 cGy) and a single dose of 15 cGy ^{56}Fe ions in the Bragg peak plateau region. The average dose rate for the ^{1}H and ^{56}Fe irradiations was ~16 ± 4 cGy/min and ~13 ± 2 cGy/min, respectively. After irradiation, all animals were delivered from BNL to GeneSys Research Institute for long-term housing during the course of the study and experimental analysis. Nonirradiated control mice underwent identical procedures; they were placed in polystyrene boxes, brought inside the cave at the NSRL facility and placed on the platform, but no beam line was administered.

Experimental Groups

We evaluated the effect of different sequences of fractionated sequential low-dose whole-body 17 cGy ^{1}H (1 GeV) and a single dose of 15 cGy ^{56}Fe (1 GeV/nucleon) radiation-induced biological response in the hearts of 8–10-month-old (at the time of initial irradiation) C57BL/6NT mice at 1 and 3 months postirradiation. The study was comprised of four groups:

- group 1, nonirradiated controls;
- group 2, three fractionated doses of 17 cGy ^{1}H every other day (^{1}H × 3);
- group 3, three fractionated doses of 17 cGy ^{1}H every other day followed by a single low dose of 15 cGy ^{56}Fe two days after the final ^{1}H dose (^{1}H × 3 + ^{56}Fe); and
- group 4, a single low dose of 15 cGy ^{56}Fe followed (after 2 days) by three fractionated doses of 17 cGy ^{1}H every other day (^{56}Fe + ^{1}H × 3).

Radiation Group

The effects of low-dose, whole-body irradiation on the heart, administered using different sequential treatments and radiation-induced alterations in cardiac function, tissue, cellular and molecular changes in aging groups at 1 and 3 months postirradiation, were assessed by echocardiography (ECHO) and hemodynamics (HEMO). In addition, cardiac fibrosis was assessed by Masson's trichrome and hematoxylin and eosin (H&E) staining and activation of signaling pathways by protein analyses.

Radiation with Myocardial Infarction Group and Acute Myocardial Infarction Surgery

We examined the effect of low-dose whole-body irradiation on the hearts of 8–10-month-old C57BL/6NT mice at 1 month after different radiation sequential treatments (described above) in a MI model. Myocardial infarction was induced by ligation of the left anterior descending coronary artery at 1 month postirradiation, as previously described elsewhere (*42, 43*) and mice were monitored for 28 days after MI using ECHO, prior to sacrificing HEMO measurements were performed on day 28.

Cardiac Physiology

Echocardiography. After measurement of body weight, animals were lightly anesthetized with isoflurane vaporized in O_2 (1.5–2%) at the rate of 1 L/min using a nose cone on a warming pad. Two-dimensional guided M-mode ECHO was performed with a 15-MHz (15–6L) pediatric open heart surgery transducer (Agilent Technologies Inc., Santa Clara, CA) as detailed in earlier published work (*44*). At least 5 sequential beats were analyzed (n = 6–8/group). Heart rate, left ventricular (LV) end-diastolic diameter (EDD), end-systolic diameter (ESD) and LV wall thickness were measured.

Left ventricular ejection fraction percentage was calculated using a standard formula with end-diastolic volume (EDV) and end-systolic volume (ESV): ejection fraction percentage = [(EDV – ESV)/EDV] × 100.

Fractional shortening percentage was calculated using the standard formula: fractional shortening percentage = [(EDD – ESD)/EDD] × 100. All ECHOs were performed by a single investigator (JL), read by a single investigator (RM) and re-read by his clinical attending (JPM); all three were blinded to the treatment conditions. ECHO data analyses were performed by a single investigator (XY) who was also blinded to the treatment conditions. Only after completion of all analyses and data plotting, were treatment conditions revealed to all investigators.

Hemodynamics. *In vivo* LV pressure measurements were performed by direct LV catheterization using Millar Mikro-Tip® Blood Pressure System (1.2 F; Transonic Systems Inc./Scisense, Ithaca, NY) (n = 6–8/group) as detailed previously (*44*). Heart rate, LV systolic pressure (LVSP), LV end-diastolic pressure (LVEDP), dP/dt_{max} and dP/dt_{min} were recorded.

Histology, Imaging and Analysis

Routine histology, H&E staining. Sections (10 μm) of formalin-fixed, paraffin-embedded heart tissue were H&E stained and visualized using a light microscope (Leica Microsystems Inc., Buffalo Grove, IL). Images of the full circumference of the heart cross sections along with the infarction area after MI were taken at 100× magnification and collaged.

Radiation-induced fibrosis, Masson's trichrome staining. To determine whether different sequences of fractionated sequential low-dose ^{1}H- and single-dose ^{56}Fe radiation could induce cardiac fibrosis 1 and 3 months postirradiation, serial 10 μm sections of cardiac tissue were processed for Masson's trichrome staining (Electron Microscopy Sciences, Hatfield, PA) and random regions of the heart were imaged at 200× (n = 20 images/sample per group) for analysis using the ImageJ program version 1.40 (NIH, Bethesda, MD) for quantification of fibrosis (blue pixels). Analyses were performed by two investigators (J. S. and H. E.) independently of each other and both were blinded to the treatment conditions.

In addition, at 28 days after MI, analysis was performed on full-circumference bright-field microscopic images (100×) of at least 40–50 cross sections of the right and left ventricles along with the infarction region of heart, using ImageJ software to quantify infarction size as previously described elsewhere (*45*). As before, these analyses were performed by two investigators (JS and HE) independently of each other and both were blinded to the treatment conditions.

Western Blot Analysis

To evaluate signaling pathways that regulate cardiac functions after irradiation and MI at the 1-month time point, we performed Western blot analysis at different time points. LV tissue (n = 3–5/treatment group) at different times postirradiation (1 and 3 months) and after MI (3, 7, 14 and 28 days) were snap-frozen in liquid nitrogen immediately after collection. LV tissue was homogenized using tissue homogenizer in a buffer containing 20 m*M* Tris (pH 7.5), 150 m*M* NaCl, 1 m*M* EDTA, 1 m*M* EGTA, 1% Triton™ X-100, 10 m*M* sodium pyrophosphate, 20 m*M* β-glycerophosphate, 10 m*M* Na_3VO_4, 1 m*M* NaF, 1 m*M* PMSF and protease inhibitor cocktail tablet (Roche Diagnostics, Indianapolis, IN). Samples containing 50 μg of total protein from the LV tissue lysates were mixed with equal volume of 2× sample buffer and boiled for 5 min at 95°C. Protein fractions were then separated by electrophoresis on 8, 10 or 15% polyacrylamide gel

(Bio-Rad® Laboratories Inc., Waltham, MA) and blotted onto PVDF membrane. Detection of total VEGF-A and total and phosphorylated protein levels of Akt (serine 473; Ser473) and Erk1/2 were performed using antibodies against phospho-specific or total-specific antibodies (Cell Signaling Technology® Inc., Danvers, MA). Detection of total and phosphorylated protein levels of nuclear factor of activated T cells, cytoplasmic, calcineurin-dependent 4 (NFATc4) was performed using rabbit polyclonal antibodies (Santa Cruz Biotechnology® Inc., Dallas, TX) and HRP-linked goat anti-rabbit GAPDH (1:40,000 dilution; EMD Millipore, Billerica, MA) and anti-Actinin antibody (1:1,000 dilution; Abcam®, Cambridge, MA) expression was used to adjust the protein loading. Protein levels were revealed using enhanced chemiluminescence Western blotting (ECL; Fisher Scientific™, Pittsburgh, PA). Densitometry analysis of the Western blot band brightness was used to obtain total and phosphorylated levels of a protein. ImageJ software was used to measure the band intensities for each respective sequence of phosphorylated and total protein, and corresponding loading control.

Statistical Analysis

Results in all graphs are expressed as mean ± SEM. Statistical analyses were performed using one-way analysis of variance (ANOVA) followed by Fisher's LSD post hoc test StatView (SAS Institute Inc., Middleton, MA). In addition, we performed Newman-Keuls and Bonferroni-Dunn analyses to correct for multiple comparisons. Differences were considered significant at $P < 0.05$.

RESULTS

Fractionated Mixed Ion Radiation Treatments ($^{56}Fe + {}^{1}H \times 3$) Affects Cardiac Structure and Function at 3 Months Postirradiation

Short-term irradiation and aging studies at 1 and 3 months postirradiation in four cohorts (n = 60 middle-aged mice/treatment group) were performed to evaluate radiation-induced alterations in cardiac functions using ECHO and HEMO measurements; cardiac hypertrophy signaling activation was assessed using Western blot analyses (Fig. 1A).

Cardiac physiology and fibrosis. ECHO and HEMO studies showed that at 1 month postirradiation, ejection fraction percentage from the hearts of group 3 was slightly decreased compared to all other groups, which had normal ejection fraction percentages (Fig. 1B). At 3 months postirradiation, all groups exhibited comparable ejection fraction percentages (Fig. 1B). There were no noticeable differences between the controls and any of the irradiated groups at 1 and 3 months in LV posterior wall thickness (Fig. 1C) or in LV end-systolic pressure (Fig. 1D). LV end-diastolic pressure at 1 month postirradiation was comparable among all four groups (Fig. 1E). However, dP/dt_{max} was decreased in the hearts of group 4 (Fig. 1F) compared to group 3, but not compared to controls or group 2 hearts, suggesting a reduced cardiac contractile function at 1 month postirradiation in group 4. Compared to all the other groups, cardiac fibrosis was increased in group 4 at 3 months postirradiation (Fig. 1G), which was associated with significant increase in LV end-diastolic pressure in the same group (Fig. 1E), indicating the development of cardiac hypertrophy, perhaps compensatory.

Candidate signaling mechanisms. To determine underlying molecular mechanisms that may be responsible for changes in cardiac function at 1 and 3 months postirradiation, we evaluated the expression and activity of proteins that are involved in the regulation of calcium handling and hypertrophy in all four groups. Expression of sodium calcium exchanger, a protein critical for proper calcium handling (*46*), was unchanged between the controls and groups 2–4 at both 1 and 3 months postirradiation (data not shown). To assess activation and onset of cardiac hypertrophy we evaluated the levels of phosphorylated NFATc4 in heart tissue. We found that there were no considerable differences in the expression of NFATc4 phosphorylation in the hearts of groups 2–4 compared to controls at 1 month postirradiation (Fig. 2A and B). However, the hearts from group 4 showed significantly decreased phosphorylation of NFATc4 at 3 months postirradiation (Fig. 2C and D), suggesting activation of cardiac hypertrophy signaling. Taken together, the increased LV end-diastolic pressure, increased cardiac fibrosis and activation of cardiac hypertrophy signaling in group 4 hearts, indicate that a single low dose of ^{56}Fe ions followed by multiple low doses of ^{1}H radiation has significant negative effects on cardiac structure and function, unlike the other treatment regimens tested here.

Fractionated Mixed Ion Radiation Treatments ($^{1}H \times 3 + {}^{56}Fe$) Increase Post-MI Mortality and Attenuates Cardiac Recovery at 1 Month Postirradiation

To evaluate the effect of fractionated mixed ion radiation on cardiac tissue recovery and regeneration after MI, we ligated the left anterior descending coronary artery at 1 month postirradiation. Figure 3A shows post-MI mortality, cardiac function, remodeling and molecular signaling, which were examined by ECHO, HEMO, Masson's trichrome staining and protein analyses. As shown in Fig. 3B, at 1 month after MI (n = 15–17 mice/treatment group; P = ns), survival analysis showed 100% survival in group 1 (black) and group 2 (green), while there was ~78% and 92% survival in group 3 (blue) and group 4 (red), respectively.

Cardiac physiology. No significant difference was observed in ejection fraction percentages among all four groups at 28 days after MI (Fig. 3C). With the exception of group 4, the LV posterior wall thickness at day 28 after MI for all other groups were comparable to those before MI (Fig. 3D). Although the LV posterior wall thickness was significantly increased in group 4 (Fig. 3D) at day 28 after MI, other cardiac output functions were comparable to the heart tissue from control post-MI group (Fig. 3E–G). In group 3, HEMO analysis at day 28 after MI revealed significantly decreased LV end-diastolic pressure (Fig. 3F) and reduced LV end-systolic pressure, suggesting that in the group 3 survivors, the functional recovery after MI is significantly diminished. Although compared to all other

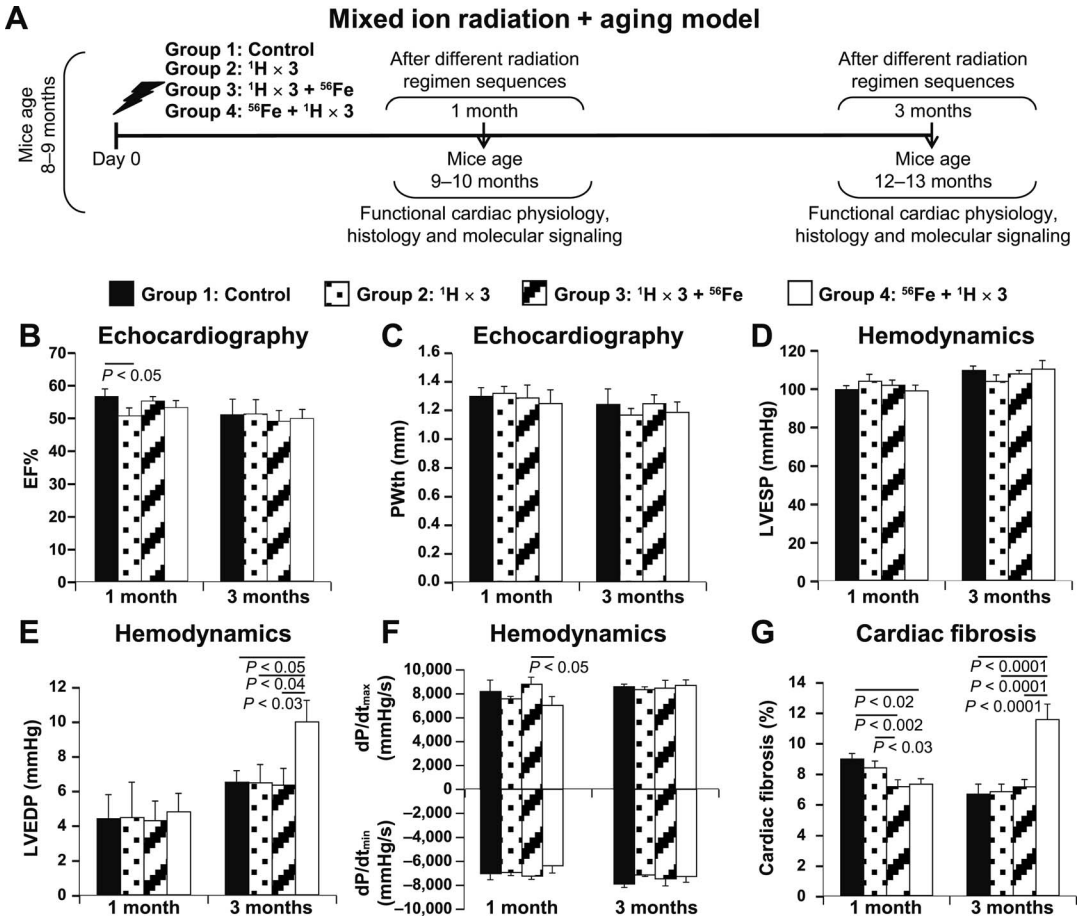

FIG. 1. ECHO and HEMO measurements of cardiac functions and evaluation of cardiac fibrosis in a radiation and aging mouse model. Panel A: Experimental design to evaluate the effect of different sequences of whole-body fractionated low-dose 17 cGy, 1 GeV ^{1}H and a single dose of 15 cGy, 1 GeV/nucleon ^{56}Fe radiation in the hearts of 8–10-month-old C57BL/6NT mice over 1 and 3 months postirradiation. Radiation-induced alterations in the radiation and aging model in cardiac function were assessed by echocardiography (ECHO), hemodynamic (HEMO), morphometric/histologic measurements and activation of signaling pathways by protein analyses. ECHO analysis of cardiac function: ejection fraction (EF%) (panel B) and posterior wall thickness (PWth) (mm) (panel C). HEMO measurements and analysis of cardiac function at 1 and 3 months postirradiation: LV end-systolic pressure (LVESP) (mmHg) (panel D); LV end-diastolic pressure (LVEDP) (mmHg) (panel E); LV dP/dt_{max} and dP/dt_{min} (mmHg/s) (panel F). Panel G: Graphic representation of fibrosis percentage in the hearts of different radiation treatment sequences of whole-body irradiated and nonirradiated control mice at 1 and 3 months postirradiation, evaluated with Masson's trichrome staining. Results in all graphs (panels B–G) are presented as mean ± SEM (n = 6–8 animals per time point/group). Group 1: nonirradiated control (solid black bars); group 2: $^{1}H \times 3$ irradiation (dotted bars); group 3: $^{1}H \times 3 + {}^{56}Fe$ irradiation (diagonal line bars); and group 4: $^{56}Fe + {}^{1}H \times 3$ irradiation (clear bars). Statistical significance was assigned when $P < 0.05$.

treatment groups, the tissues from group 3 showed a trend of decreased dP/dt_{max} and $dP/dt_{min,}$ (Fig. 3G), these changes were not statistically significant. Evaluation of cardiac remodeling after MI using Masson's trichrome staining revealed that the hearts from group 3 had significantly larger infarction size compared to controls and irradiated MI groups (Fig. 3H and I). This data along with decreased LV end-systolic pressure (Fig. 3E) and LV end-diastolic pressure (Fig. 3F) further highlights the deleterious effects of $^{1}H \times 3 + {}^{56}Fe$ exposures on cardiac functional and structural recovery at 2 months postirradiation and at 1 month after MI.

Candidate signaling mechanisms. To understand the divergent responses to different sequence and fractionation of mixed ion radiation, we examined the underlying signaling molecules, such as VEGF-A, Akt (Ser473) and Erk1/2 (*47–49*), which regulate angiogenesis, survival, proliferation of cardiac tissue damage recovery and remodeling on days 3 and 7 after MI. On day 3 after MI, the levels of VEGF-A and phosphorylated (phospho-) p-Erk1/2 were essentially maintained and comparable (data not shown). However, the phosphorylation of Akt (at Ser473) at day 3 after MI was significantly lower in all irradiated + MI treatment groups compared to the control + MI groups (data not shown). At day 7 post-MI, compared to control animals, we observed substantial increase in the levels of VEGFA (Fig. 4A and B) and p-Erk1/2 (Fig. 4C and D) in MI treatment groups 2 and 4, while levels of these proteins found in group 3 were comparable to control levels. The expression of p-Akt (Ser473) remained significantly reduced in all irradiated + MI hearts compared to the control + MI group (Fig. 4E and F). These findings reveal a

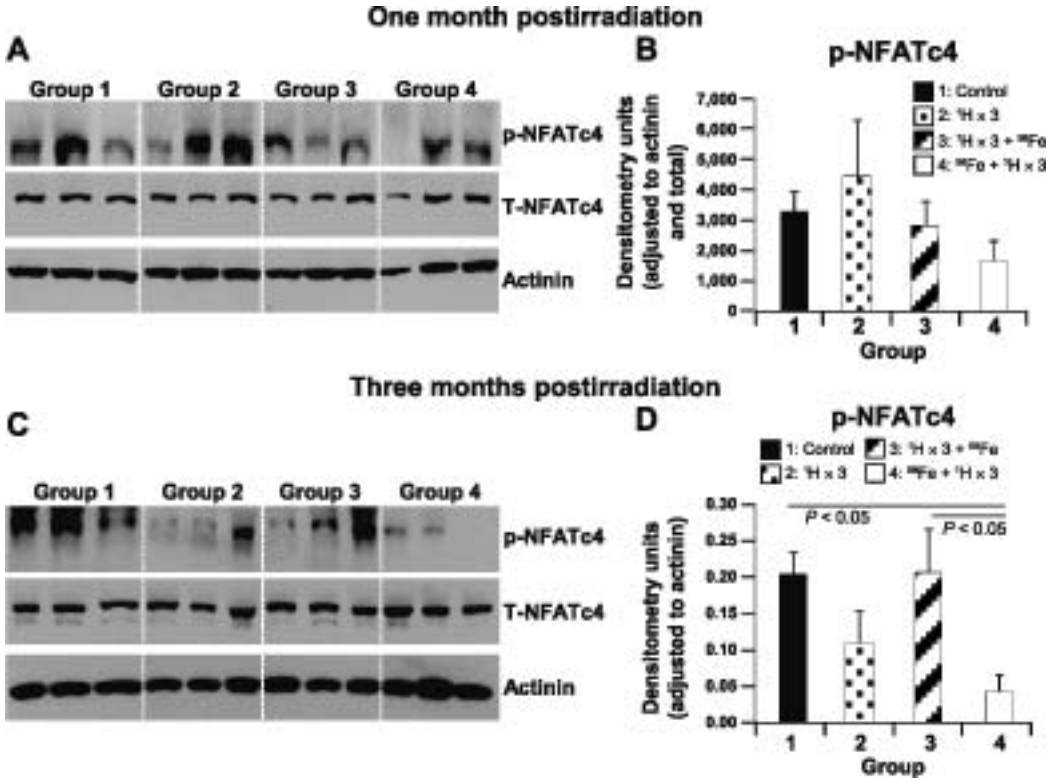

FIG. 2. Radiation-induced changes in signaling pathways at 1 and 3 months postirradiation. Representative Western blots of heart tissue homogenates from radiation and aging mouse models, groups 1–4 (nonirradiated controls; $^{1}H \times 3$; $^{1}H \times 3 + {}^{56}Fe$; and $^{56}Fe + {}^{1}H \times 3$. Bands represent phosphorylated (p), total (T) and loading control for the following proteins: p-NFATc4, T-NFATc4 (140–150 kDa) and actinin (103 kDa), at 1 and 3 months postirradiation (panels A and C, respectively). Quantification and graphic representation of total protein levels and phosphorylation using densitometric analysis of phospho-band intensities after adjusting for corresponding actinin and total band intensities of heart tissue homogenates for p-NFATc4, at 1 and 3 months postirradiation (panels B and D, respectively). Results in all graphs represent mean ± SEM (n = 6–8 animals per time point/group). Group 1: nonirradiated control (solid black bars); group 2: $^{1}H \times 3$ irradiation (dotted bars); group 3: $^{1}H \times 3 + {}^{56}Fe$ irradiation (diagonal line bars); and group 4: $^{56}Fe + {}^{1}H \times 3$ irradiation (clear bars). Statistical significance was assigned when $P < 0.05$.

complex mixed ion radiation-mediated spatial and temporal regulation of VEGFA, p-Erk1/2 and p-Akt in irradiated + MI hearts and suggest that decreases in all three of these protein levels and activity may be responsible, at least in part, for the attenuated cardiac recovery and regeneration in the MI group 3.

DISCUSSION

Earlier reports on assessments of space radiation risks and acceptable levels of cardiovascular risk were largely focused on LEO missions (*19*), which are not entirely relevant for deep-space missions due to the uncertainties associated with complex variations in the GCR and SPE spectra and the lack of information on the radiobiological responses to HZE ions in the GCR and SPE-like proton particles (*3, 16, 17*). Such a dubious backdrop has resulted in numerous published studies over the past two decades in cell- and animal-based models using protracted, low-dose-rate HZE ion, neutron and proton exposures with a broad spectrum of energy ranges, which mimic the deep-space environment and its impact on various biological systems, to estimate both short- and long-term risks and reduce uncertainties (*15, 50*). These studies have clearly demonstrated both qualitative and quantitative differences in biological response to HZE particle radiation when compared to terrestrial radiation. Immune system suppression and acute hematological effects in the form of reduced number and functionality of circulating leukocytes (white blood cells; WBC), erythrocytes (red blood cells; RBC) and platelets have been associated with combination treatment of SPE-like ^{1}H radiation exposure with or without hindlimb unloading in mice (*51–54*). When this data is cautiously translated to astronauts, such deficiencies can result in acute radiation effects such as weakened immune system with altered cytokine production (*55*), increased risks of developing infections (*56*), blood cell death and thrombotic diseases for which countermeasures are being evaluated.

Along with acute effects of radiation, other biomedical risks of significant concern with a long-duration space mission are radiation carcinogenesis, acute and late effects of radiation on the central nervous system and degenerative

tissue systems (*3, 7, 9, 14, 15, 18*) including heart, circulatory system, lung, bone, muscle, endocrine, digestive and lens, to name a few (*9*). Acute exposure of mice to ^{16}O (30 cGy) and ^{48}Ti (5 and 30 cGy) particle radiation showed severe decrements in cognitive behavior and neural dysfunction by 6 weeks postirradiation (*6*), which corroborated with similar findings of significantly impaired memory and learning, as well as neural cell death after exposure to low-dose ^{56}Fe particles (20 cGy) (*57, 58*) in a rodent model. Published ground-based studies of rodent models using hindlimb unloading with or without radiation (both terrestrial and HZE particles) show well documented musculoskeletal disuse bone loss (*59–62*), as well as skeletal microarchitectural changes (*63, 64*) normally associated with onset of age-related osteoporosis.

Direct or indirect outcomes of radiation-induced damage on biomolecules as well as cellular structures in the form of mutations, DNA damage, cell death, phenotypic changes and increased oxidative stress levels (*21*) can exacerbate the risk of degenerative diseases (e.g., cardiovascular and circulatory) that are usually associated with aging (*3*). While the intracellular effects of HZE radiation, such as DNA damage and repair (*65, 66*), persistent oxidative stress (*67*) and cell cytotoxicity (*68*), have been studied, comprehensive work to elucidate how HZE particles affect heart tissue and cardiac function is still in its infancy. Previously published studies have highlighted the acute effects of high-dose radiation in cardiomyocytes (*69, 70*) with the primary focus on upregulation of gene transcription (*71*). We recently reported on the long-lasting, cyclical, time-dependent change observed in gene regulation in left ventricular cardiomyocytes up to 28 days after a single whole-body low-dose 15 cGy ^{56}Fe exposure (*72*). We reported a cyclical increase in the activity of inflammatory and free radical scavenging genes, as well as modulation of transcription factors STAT-3, GATA-4, TBX5, MEF2c, NFATc4 and NF-κB that are required for the maintenance of cardiac morphogenesis, myogenesis, vascular development and protection from pressure overload-induced heart failure, were activated (*73*). In an earlier study, we also reported increased DNA damage with slow decay of DNA double-strand breaks in cardiomyocytes up to 28 days postirradiation, as well as cyclical inflammatory response in the heart tissue over an extended period of 10 months after whole-body 15cGy ^{56}Fe irradiation (*40*). Taken together, these findings further signify a possible and potential feedback mechanism of ionizing radiation, perpetuating inflammatory responses in the heart that may lead to significant alterations in CV physiology and negatively affect cardiac functions, thus increasing the overall risk for CV disease development after a single low-dose space-type radiation exposure (*40, 73*). The effects of low-dose fractionated mixed ion space-type radiation on cardiac structure and function are not known. In the current study, we examined the effect of low-dose fractionated mixed ion radiation on cardiac structure and function in a model of radiation with aging, and cardiac structure, function, recovery and remodeling in a model of radiation with induced MI.

Mixed Ion Fractionated Radiation Treatment Groups. In our studies, animal groups exposed to fractionated low doses of protons (group 2; $^{1}H \times 3$) and mixed ions (group 3; $^{1}H \times 3 + ^{56}Fe$) showed no negative effect on cardiac function up to 3 months postirradiation, when compared to nonirradiated controls. Radiation-induced deleterious effects on cardiac function were first observed in treatment group 4 ($^{56}Fe + ^{1}H \times 3$), in the form of significant and depressed dP/dt_{max} compared to hearts from group 3, suggesting an alteration in contractile function as early as 1 month postirradiation. This early hemodynamic alteration of cardiac function in the group 4 mouse hearts was later manifested by considerably increased LV end-diastolic pressure and cardiac fibrosis compared to all other treatment groups at 3 months postirradiation (Fig. 1E–G). Studies have shown that increased LV end-diastolic pressure is known to develop cardiac hypertrophy due to a continuous need to pump more and more blood (*74*), and an increase in cardiac fibrosis is known to develop as concentric hypertrophy (*75*). Yet, the lack of increase in LV posterior wall thickness to compensate for increase in LV chamber radius leads to progressive increase of diastolic stress that begets cardiac remodeling (*76*), eventually manifesting as increased morbidity and mortality. Therefore, taken together, our findings at 3 months postirradiation may be predictive for the development of a clinical condition known as diastolic heart failure (*77*) which is characterized by diastolic dysfunction (*78*), concentric LV hypertrophy and normal ejection fraction percentage (*77*).

Cardiac hypertrophy, a compensatory mechanism of the heart when exposed to stressors, is well known to be regulated by the transcription factor NFATc4 (*79, 80*). Dephosphorylation of NFATc4 results in increased activation associated with adult cardiac hypertrophy (*80*), while under basal unstimulated conditions NFATc4 remains highly phosphorylated and inactive (*81*). Not surprisingly, we observed significant activation of NFATc4 in the mouse hearts of group 4 ($^{56}Fe + ^{1}H \times 3$), indicating activation of cardiac hypertrophy signaling at 3 months postirradiation. The increased NFATc4 activation in group 4 mouse hearts 3 months postirradiation might support a mechanism for cardiac contractile dysfunction resulting in increased morbidity (*82, 83*) owing to increased LV end-diastolic pressure and increased cardiac fibrosis due to increased LV afterload.

Taken together, our findings in a model of radiation with 3-month follow-up demonstrate that a single low dose of 15 cGy, 1 GeV/nucleon of ^{56}Fe ion radiation followed by three doses of 17 cGy, 1 GeV of ^{1}H induced cardiac hypertrophy and diastolic dysfunction accompanied by increased cardiac fibrosis at 3 months postirradiation. However, an approximately equitoxic total dose of 50 cGy, 1 GeV ^{1}H-particle radiation delivered in three equal sequential fractions, as in group 2 ($^{1}H \times 3$), or a different sequence of three ^{1}H fractions followed by a single ^{56}Fe dose, as in group 3 ($^{1}H \times 3 + ^{56}Fe$), had no negative effect on the heart over 3 months postirradiation. This finding suggests the possibility that ^{1}H

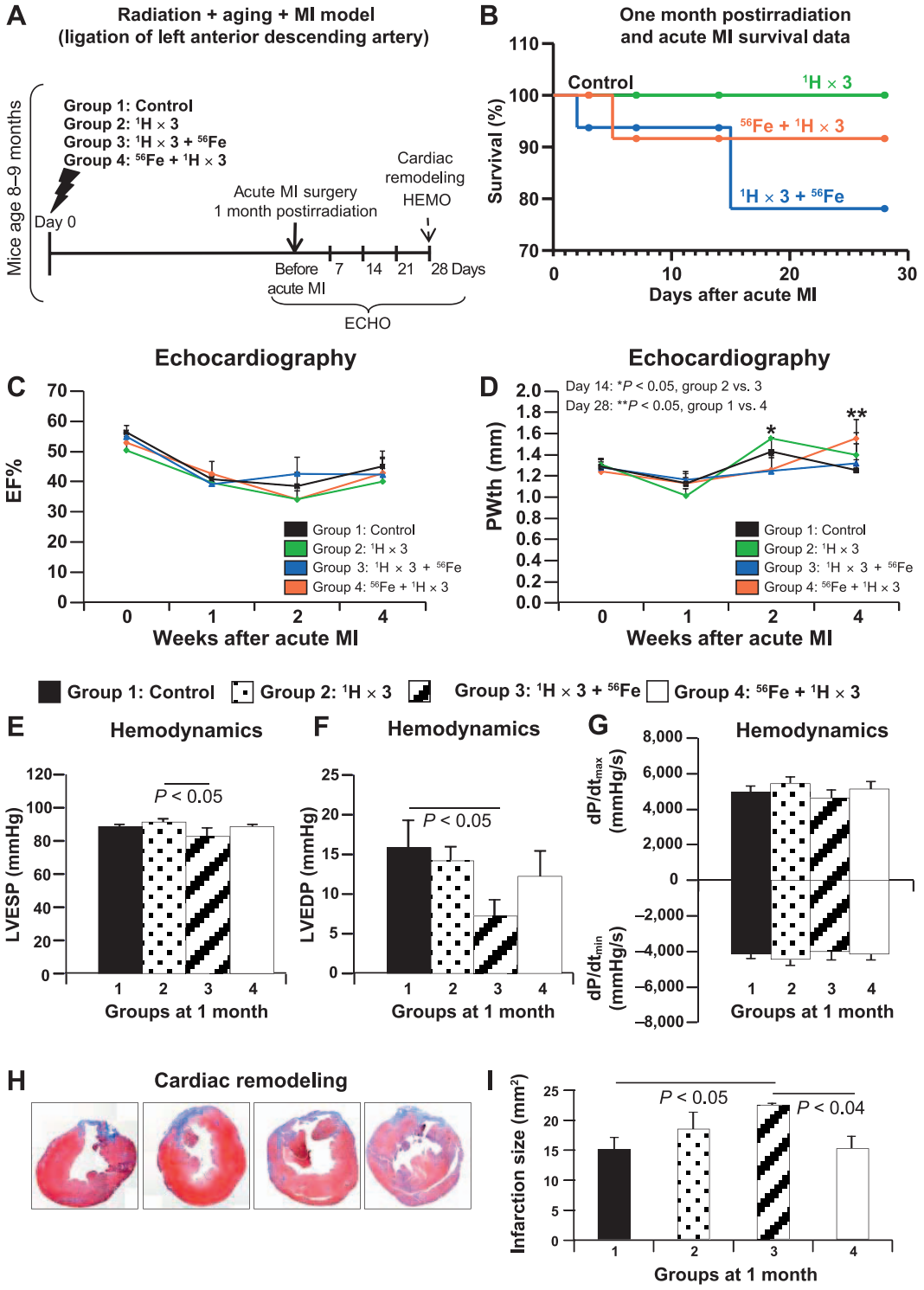

FIG. 3. ECHO, HEMO measurements of cardiac functions and cardiac remodeling in the radiation and aging plus MI model. Panel A: Experimental design to evaluate the effect of different sequences of whole-body fractionated low-dose 17 cGy, 1 GeV ^{1}H and a single dose of 15 cGy, 1 GeV/nucleon ^{56}Fe radiation in the hearts of 8–10-month-old C57BL/6NT mice at 1 month postirradiation. Radiation-induced alterations in cardiac function were assessed by echocardiography (ECHO), hemodynamic (HEMO) and morphometric/histologic measurements and activation of signaling pathways by protein analyses. Acute MI was induced by ligation of the left anterior descending coronary artery at 1 month postirradiation, and mice were monitored for 28 days after MI. Panel B: Post-MI survival data. ECHO analysis of cardiac function at 1 month postirradiation in mice for ejection fraction (EF%) and posterior wall thickness (PWth) (mm) (panels C and D, respectively). Results in all graphs (panels C and D) are presented as mean ± SEM (n = 6–8 animals per time point/group). Group 1: nonirradiated control (solid black line); group 2: ^{1}H × 3 irradiation (solid green line); group 3: ^{1}H × 3 + ^{56}Fe

radiation, delivered in three low-dose fractions, might prime the heart to respond better to a subsequent single low dose of the more damaging ^{56}Fe radiation, and help maintain the cardiac functions postirradiation. The precise mechanism(s) for this type of priming effect are not known. However, if we take a DNA damage- and repair-centric view, it may be related to enhancement of DNA damage repair capacity (i.e., inducible or adaptive response) by small doses of ^{1}H prior to ^{56}Fe irradiation (*84, 85*). Another possible mechanism could be a direct priming effect on heart tissue through activation of anti-apoptotic and anti-oxidative pathways, which might improve cardiac function and inhibit hypertrophic remodeling, as reported in a diabetic cardiomyopathy model (*86*). It is worth noting here that the activation of cardiac hypertrophic signaling (NFATc4 activation) after irradiation with ^{56}Fe followed by $^{1}H \times 3$ might serve as a compensatory mechanism for preserving cardiac functions but could become detrimental over longer periods time, resulting in augmentation of cardiac dysfunction and ultimately lead to the development of heart failure (*87–89*). Longitudinal studies are required to confirm this hypothesis.

Radiation and Myocardial Infarction Treatment Groups. We evaluated the effect of different low-dose sequential fractionated ^{1}H and ^{56}Fe ion treatments on the recovery of the heart in a well-established ischemic model of induced myocardial infarction (MI). We observed no detrimental effects on post-ischemic recovery in the MI model in the nonirradiated controls nor in animals exposed to three ^{1}H fractions ($^{1}H \times 3$) at 1 month postirradiation. However, a single low dose of ^{56}Fe prior to sequential fractionated ^{1}H irradiation (group 4) offered a different scenario compared to the similar radiation treatments in the aging model. Apart from a small increase in post-MI mortality rate (9%), compared to control (group 1) and $^{1}H \times 3$ (group 2) irradiated mice, all the other functional and morphological readouts were not affected in group 4 animals. In the radiation with MI treatment model, contrary to the mixed ion radiation model, fractionated ^{1}H followed by a single low dose of ^{56}Fe radiation (group 3) induced substantial negative effects on post-MI recovery. These included significant decreases in systolic and diastolic functions in the form of reduced LV end-diastolic pressure and LV end-systolic pressure along with the trend of decreased dP/dt_{max} and dP/dt_{min}, thinner LV posterior wall thickness and larger infarction size. Taken together, our findings in the radiation versus radiation with MI treatment models suggest significant mixed ion fractionation and sequence-dependent divergent responses in the heart during aging and after an ischemic CV event.

To assess possible underlying molecular signaling involved in cardiac remodeling we examined key molecules in angiogenic, survival and proliferative signaling pathways 3 and 7 days after MI. No difference in VEGF-A and Erk1/2 expression was observed as early as 3 days after MI in all study groups, whereas expression of Akt (Ser473), a prosurvival signaling molecule, was downregulated in all irradiated groups compared to control hearts.

Two well-characterized signaling protein kinases are required for restoration of cardiac functions after MI: Erk1/2, which regulates inflammation and apoptosis (*90*); and Akt, which has an essential role in survival signaling and reduction of inflammation (*48*). The combination of upregulation of VEGF-A expression and activation of Akt, and Erk1/2 is imperative for proper recovery and repair after MI (*91, 92*), and ultimately, in the cardiac remodeling with minimal scar tissue formation (*93*). The decreases observed in Akt (Ser473) expression as early as day 3 that continued to day 7 after MI, combined with decreases in the expression of VEGF-A and activation of p-Erk1/2 (*47*) on day 7, may be partially responsible for the worsened cardiac function observed in MI hearts exposed to $^{1}H \times 3$ followed by ^{56}Fe radiation (*94, 95*) but not in the other irradiated groups, in which VEGF-A was upregulated and p-Erk1/2 was activated at day 7. Conversely, the reduced expression of Akt (Ser473) signaling in MI mouse hearts in treatment groups 2 ($^{1}H \times 3$) and 4 ($^{56}Fe + {}^{1}H \times 3$) at day 7 after MI, even though not favorable for efficient MI recovery, was partially improved by increased signaling through Erk1/2 and VEGF-A, thus ensuring improved cardiac function and smaller infarction scar tissue at day 28 after MI.

It is immeasurably important to determine possible factors that may increase CV degenerative risks due to mixed ion low-dose ionizing particle radiation in space to develop mitigating factors for reduction of excess CV risks and to maintain cardiac homeostasis after an inevitable radiation exposure during future space missions.

←
irradiation (solid blue line); group 4: $^{56}Fe + {}^{1}H \times 3$ irradiation (solid red line). HEMO measurements and analysis of cardiac function at 1 month postirradiation in a radiation and aging plus MI model for LV end-systolic pressure (LVESP) (mmHg), LV end-diastolic pressure (LVEDP) (mmHg) and LV dP/dt_{max} and dP/dt_{min} (mmHg/s) (panels E–G, respectively). Cardiac remodeling at 1 month postirradiation and day 28 after MI was measured using Masson's trichrome staining (panel H), where blue indicates fibrosis, e.g., the infarction remodeling. Measurements represent midline length of the infarction when >50% of the LV was involved (mm) and every third section of the adjacent 8-μm-size section was measured and infarction size was reconstructed as described above. Insets (panel H) are representative images of nonirradiated control mice and mice that were whole-body irradiated using different sequences. Panel I: Graphic representation of the infarction size/scar (mm^2) at 1 month postirradiation and 28 days after MI. Results in all graphs (panels C–G, I) are presented as mean ± SEM (n = 6–8 animals per time point/group). Statistical significance was assigned when $P < 0.05$.

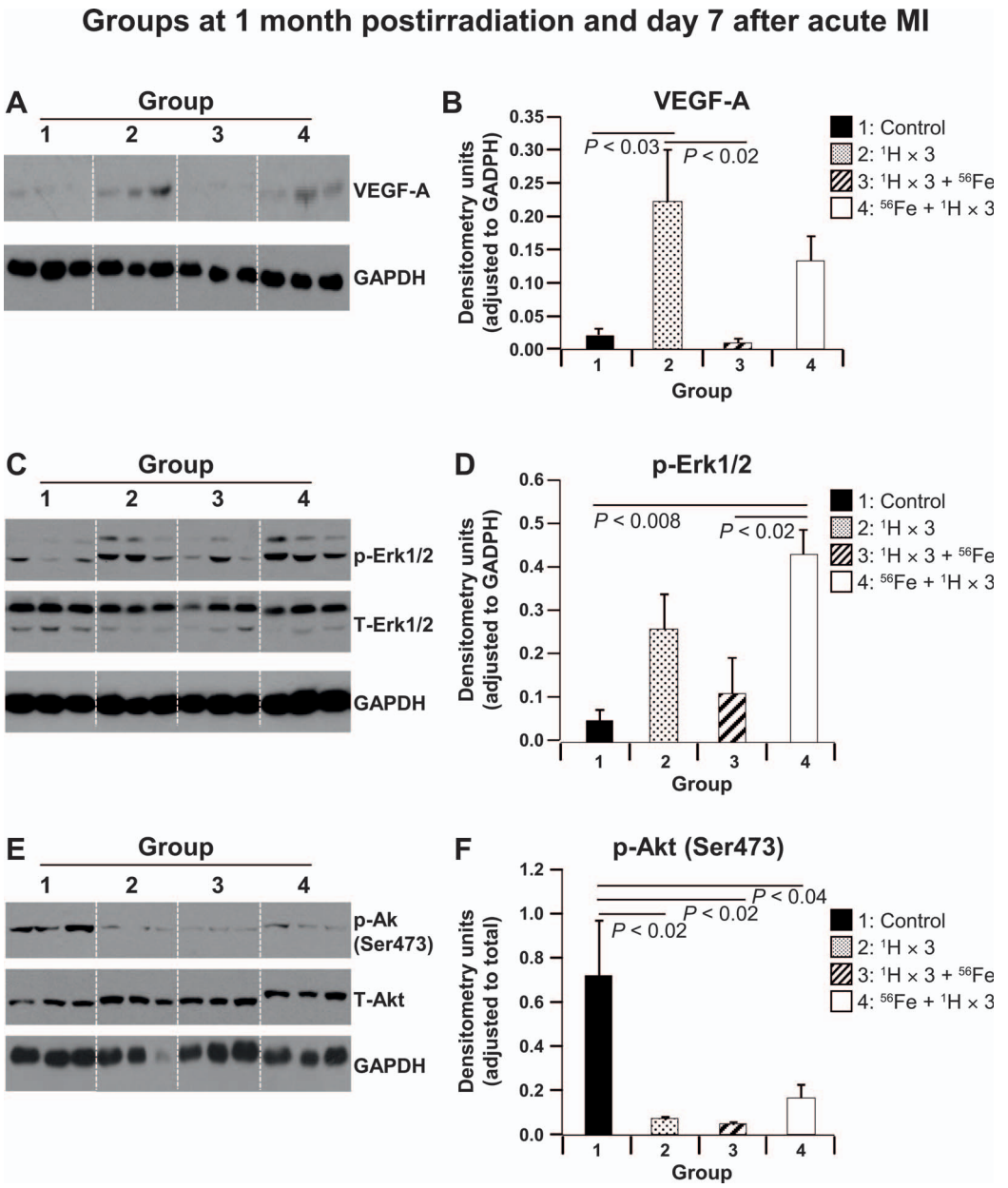

FIG. 4. Protein analyses at 1 month postirradiation and 7 days after MI. Representative Western blot images of heart tissue homogenates from nonirradiated control mouse hearts and hearts of mice that were whole-body irradiated using different sequences at 1 month postirradiation in a radiation and aging plus MI model. Images represent scans of radiograms for phosphorylated (p), total (T) and loading control on day 7 for the following proteins: VEGF-A (38 kDa) and GAPDH (panel A); p-Erk1/2, T-Erk1/2 (42/44 kDa) and GAPDH (panel C); p-Akt (Ser473), T-Akt (62 kDa) and GAPDH (panel E). Quantification and graphic representation of total protein levels and phosphorylation using densitometric analysis of phospho-band intensities after adjusting for corresponding GAPDH (36 kDa) and total band intensities of heart tissue homogenates at 1 month postirradiation in a radiation and aging plus MI model for the following proteins: VEGF-A, p-Erk1/2 and p-Akt (Ser473) (panels B, D and F, respectively). Group 1: nonirradiated control (solid black bars); group 2: $^{1}H \times 3$ irradiation (dotted bars); group 3: $^{1}H \times 3 + {}^{56}Fe$ irradiation (diagonal line bars); and group 4: $^{56}Fe + {}^{1}H \times 3$ irradiation (solid red bars). Results in all graphs are depicted as mean ± SEM (n = 6–8 animals per time point/group). Statistical significance was assigned when $P < 0.05$.

SUMMARY

In this study, we observed that in our mixed ion radiation model, up to 3 months after fractionated ^{1}H irradiation alone ($^{1}H \times 3$) or followed by a single ^{56}Fe dose ($^{1}H \times 3 + {}^{56}Fe$) did not have a significant negative effect on post-irradiated animal survival or cardiac function. In fact, both mixed ion radiation treatments decreased cardiac fibrosis, at least 1 month postirradiation. When a single ^{56}Fe fraction was followed by fractionated ^{1}H irradiation ($^{56}Fe + {}^{1}H \times 3$),

there were several negative developments: 1. Cardiac fibrosis was increased >85%; 2. LV dP/dt_{max} was decreased at 1 month, LV end-diastolic pressure (EDP) was increased at 3 months, both of which are indicative of negative hemodynamic developments in the hearts of the surviving fraction of mice.

We also observed that the MI models irradiated with either $^{1}H \times 3$ or ^{56}Fe followed by $^{1}H \times 3$ did not show a significant negative effect in post-MI survival and cardiac function at 1 month postirradiation. In the model irradiated with $^{1}H \times 3$ followed by ^{56}Fe, several negative developments occurred: 1. There was a 24% decrease in post-MI survival at 1 month; 2. LV ESP and EDP were decreased at 1 month, indicating altered contractile function; 3. Post-MI cardiac fibrosis was increased. All three findings are indicative of significant negative effects for post-MI recovery from $^{1}H \times 3$ followed by ^{56}Fe irradiation in the surviving fraction of mice in this group.

Taken together, our data suggest that low-dose mixed ion exposures of charged particles present in the space radiation environment may have a significant effect on the CV system. Furthermore, differing sequences of radiation exposure by which tissue is traversed, from the most abundant particle in the space environment (protons) and one of the most damaging HZE ions (iron), can induce dramatically different biological responses on cardiovascular system recovery under baseline conditions and after an ischemic event. These findings emphasize the necessity to determine underlying molecular mechanisms responsible for this significant mixed ion fractionation and sequence-dependent divergent responses in the heart under baseline conditions and in case of a possible ischemic cardiovascular event, such as a myocardial infarction.

We believe that these findings will provide useful information for risk analysis efforts for future NASA exploration-type space missions and aid in the development of mitigating countermeasures to reduce CV risks during long-duration deep-space missions. Our studies may also provide a foundation for the development of therapeutic measures to prevent CV morbidity and mortality due to particle cancer radiotherapy, which is becoming a more acceptable component to combined treatments in cancer therapy.

ACKNOWLEDGMENTS

We thank the following members of the Biological, Environmental and Climate Sciences Department and the Animal Facility at the NASA Space Radiation Laboratory at Brookhaven National Laboratory for their help and support of our research work: Dr. Adam Rusek, Dr. Peter Guida and MaryAnn Petry and their teams. This work was supported by NASA grant no. NNX11AD22G and the American Heart Association, grant no. 14GRNT18860032 to D. A. G. Additional support was provided in part by grants from the NIH National Heart, Lung, and Blood Institute (NHLBI), grant nos. HL106098 to X. Y. and HL091983 to R. K. The funders had no role in study design, data collection and analysis, decision to publish or manuscript preparation.

Received: October 26, 2016; accepted: April 17, 2017; published online: June 14, 2017

REFERENCES

1. Hoffman SJ, Kaplan DI. Human exploration of mars: the reference mission of the NASA Mars Exploration Study Team. National Aeronautics and Space Administration (NASA) Special Publication 6107; 1997:21–237.
2. Cucinotta FA, Kim MH, Chappell LJ, Huff JL. How safe is safe enough? Radiation risk for a human mission to Mars. PLoS One 2013; 8:e74988.
3. Chancellor JC, Scott GB, Sutton JP. Space radiation: the number one risk to astronaut health beyond low earth orbit. Life 2014; 4:491–510.
4. Task Group on Radiation Protection in Space, ICRP Committee 2, Dietze G, Bartlett DT, Cool DA, Cucinotta FA, Jia X, et al. Assessment of radiation exposure of astronauts in space. ICRP Publication 123. Ann ICRP 2013; 42:1–339.
5. Hellweg CE, Baumstark-Khan C. Getting ready for the manned mission to Mars: the astronauts' risk from space radiation. Die Naturwissenschaften 2007; 94:517–26.
6. Parihar VK, Allen B, Tran KK, Macaraeg TG, Chu EM, Kwok SF, et al. What happens to your brain on the way to Mars. Sci Adv 2015; 1:e1400256.
7. Cucinotta FA. Space radiation risks for astronauts on multiple International Space Station missions. PLoS One 2014; 9:e96099.
8. Badhwar GD, O'Neill PM. Long-term modulation of galactic cosmic radiation and its model for space exploration. Adv Space Res 1994; 14:749–57.
9. Kennedy AR. Biological effects of space radiation and development of effective countermeasures. Life Sci Space Res 2014; 1:10–43.
10. Townsend LW, Cucinotta FA, Wilson JW, Bagga R. Estimates of HZE particle contributions to SPE radiation exposures on interplanetary missions. Adv Space Res 1994; 14:671–4.
11. Reitz G. Characteristic of the radiation field in low earth orbit and in deep space. Z Med Phys 2008; 18:233–43.
12. Cucinotta FA, Nikjoo H, Goodhead DT. The effects of delta rays on the number of particle-track traversals per cell in laboratory and space exposures. Radiat Res 1998; 150:115–9.
13. Cucinotta FA, Schimmerling W, Wilson JW, Peterson LE, Saganti PB, Dicello JF. Uncertainties in estimates of the risks of late effects from space radiation. Adv Space Res 2004; 34:1383–9.
14. Cucinotta FA, Schimmerling W, Wilson JW, Peterson LE, Badhwar GD, Saganti PB, et al. Space radiation cancer risk projections for exploration missions: uncertainty reduction and mitigation. NASA JSC-29295 2001; 4–75.
15. Cucinotta FA, Alp M, Sizman F, Wang M. Space radiation risks to the central nervous system. Life Sci Space Res 2014; 2:54–69.
16. Townsend LW, Badhwar GD, Brady LA, Blakely EA, Cucinotta FA, Curtis SB, et al. Information needed to make radiation protection recommendations for space missions beyond low-earth orbit. NCRP Report No. 153. Bethesda: National Council on Radiation Protection and Measurements; 2006. p. 9–282.
17. Cucinotta FA, Schimmerling W, Wilson JW, Peterson LE, Badhwar GD, Saganti PB, et al. Space radiation cancer risks and uncertainties for Mars missions. Radiat Res 2001; 156:682–8.
18. Cucinotta FA, Durante M. Cancer risk from exposure to galactic cosmic rays: implications for space exploration by human beings. Lancet Oncol 2006; 7:431–5.
19. Fry RJM, Ainsworth EJ, Blakely EA, Boice JD, Jr., Curtis SB, Land CE, et al. Radiation protection guidance for activities in low-earth orbit. 2000; NCRP Report 132. NCRP; 17–151.
20. Hassler DM, Zeitlin C, Wimmer-Schweingruber RF, Ehresmann B, Rafkin S, Eigenbrode JL, et al. Mars' surface radiation environment measured with the Mars Science Laboratory's Curiosity rover. Science 2014; 343:1244797.
21. Willey JS, Lloyd SA, Nelson GA, Bateman TA. Space Radiation and bone loss. Gravitational and space biology bulletin: publica-

tion of the American Society for Gravitational and Space Biology 2011; 25:14–21.

22. Kim MH, Hayat MJ, Feiveson AH, Cucinotta FA. Prediction of frequency and exposure level of solar particle events. Health Phys 2009; 97:68–81.
23. Townsend LW. Implications of the space radiation environment for human exploration in deep space. Radiat Prot Dosimetry 2005; 115:44–50.
24. Hu S, Kim MH, McClellan GE, Cucinotta FA. Modeling the acute health effects of astronauts from exposure to large solar particle events. Health Phys 2009; 96:465–76.
25. Travis LB, Ng AK, Allan JM, Pui CH, Kennedy AR, Xu XG, et al. Second malignant neoplasms and cardiovascular disease following radiotherapy. J Natl Cancer Inst 2012; 104:357–70.
26. Travis LB, Ng AK, Allan JM, Pui CH, Kennedy AR, Xu XG, et al. Second malignant neoplasms and cardiovascular disease following radiotherapy. Health Phys 2014; 106:229–46.
27. Gyenes G, Fornander T, Carlens P, Rutqvist LE. Morbidity of ischemic heart disease in early breast cancer 15–20 years after adjuvant radiotherapy. Int J Radiat Oncol Biol Phys 1994; 28:1235–41.
28. Taylor CW, McGale P, Darby SC. Cardiac risks of breast-cancer radiotherapy: a contemporary view. Clin Oncol (R Coll Radiol) 2006; 18:236–46.
29. Gayed IW, Liu HH, Yusuf SW, Komaki R, Wei X, Wang X, et al. The prevalence of myocardial ischemia after concurrent chemoradiation therapy as detected by gated myocardial perfusion imaging in patients with esophageal cancer. J Nucl Med 2006; 47:1756–62.
30. Emerit I, Levy A, Cernjavski L, Arutyunyan R, Oganesyan N, Pogosian A, et al. Transferable clastogenic activity in plasma from persons exposed as salvage personnel of the Chernobyl reactor. J Cancer Res Clin Oncol 1994; 120:558–61.
31. Bose AS, Shetty V, Sadiq A, Shani J, Jacobowitz I. Radiation induced cardiac valve disease in a man from Chernobyl. J Am Soc Echocardiogr 2009; 22:973 e1–3.
32. Pant GS, Kamada N. Chromosome aberrations in normal leukocytes induced by the plasma of exposed individuals. Hiroshima J Med Sci 1977; 26:149–54.
33. Zeitlin C, Hassler DM, Cucinotta FA, Ehresmann B, Wimmer-Schweingruber RF, Brinza DE, et al. Measurements of energetic particle radiation in transit to Mars on the Mars Science Laboratory. Science 2013; 340:1080–4.
34. Convertino VA. Status of cardiovascular issues related to space flight: Implications for future research directions. Respir Physiol Neurobiol 2009; 169:S34–7.
35. Kerr RA. Planetary exploration. Radiation will make astronauts' trip to Mars even riskier. Science 2013; 340:1031.
36. Grabham P, Sharma P, Bigelow A, Geard C. Two distinct types of the inhibition of vasculogenesis by different species of charged particles. Vascular Cell 2013; 5:16.
37. Soucy KG, Lim HK, Kim JH, Oh Y, Attarzadeh DO, Sevinc B, et al. HZE (5)(6)Fe-ion irradiation induces endothelial dysfunction in rat aorta: role of xanthine oxidase. Radiat Res 2011; 176:474–85.
38. Yu T, Parks BW, Yu S, Srivastava R, Gupta K, Wu X, et al. Iron-ion radiation accelerates atherosclerosis in apolipoprotein E-deficient mice. Radiat Res 2011; 175:766–73.
39. Authors on behalf of ICRP, Stewart FA, Akleyev AV, Hauer-Jensen M, Hendry JH, Kleiman NJ, et al. ICRP publication 118: ICRP statement on tissue reactions and early and late effects of radiation in normal tissues and organs–threshold doses for tissue reactions in a radiation protection context. Ann ICRP 2012; 41:1–322.
40. Yan X, Sasi SP, Gee H, Lee J, Yang Y, Mehrzad R, et al. Cardiovascular risks associated with low dose ionizing particle radiation. PLoS One 2014; 9:e110269.
41. Murry CE, Jennings RB, Reimer KA. Preconditioning with ischemia: a delay of lethal cell injury in ischemic myocardium. Circulation 1986; 74:1124–36.
42. Zolotareva AG, Kogan ME. Production of experimental occlusive myocardial infarction in mice. Cor et Vasa 1978; 20:308–14.
43. Patten RD, Aronovitz MJ, Deras-Mejia L, Pandian NG, Hanak GG, Smith JJ, et al. Ventricular remodeling in a mouse model of myocardial infarction. Am J Physiol 1998; 274:H1812–20.
44. Ding B, Price RL, Goldsmith EC, Borg TK, Yan X, Douglas PS, et al. Left ventricular hypertrophy in ascending aortic stenosis mice: anoikis and the progression to early failure. Circulation 2000; 101:2854–62.
45. Takagawa J, Zhang Y, Wong ML, Sievers RE, Kapasi NK, Wang Y, et al. Myocardial infarct size measurement in the mouse chronic infarction model: comparison of area- and length-based approaches. J Appl Physiol 2007; 102:2104–11.
46. Shigekawa M, Iwamoto T. Cardiac Na(+)-Ca(2+) exchange: molecular and pharmacological aspects. Circ Res 2001; 88:864–76.
47. Deuse T, Peter C, Fedak PW, Doyle T, Reichenspurner H, Zimmermann WH, et al. Hepatocyte growth factor or vascular endothelial growth factor gene transfer maximizes mesenchymal stem cell-based myocardial salvage after acute myocardial infarction. Circulation 2009; 120:S247–54.
48. Vilahur G, Juan-Babot O, Pena E, Onate B, Casani L, Badimon L. Molecular and cellular mechanisms involved in cardiac remodeling after acute myocardial infarction. J Mol Cell Cardiol 2011; 50:522–33.
49. Tenhunen O, Soini Y, Ilves M, Rysa J, Tuukkanen J, Serpi R, et al. p38 Kinase rescues failing myocardium after myocardial infarction: evidence for angiogenic and anti-apoptotic mechanisms. FASEB J 2006; 20:1907–9.
50. Durante M, Cucinotta FA. Heavy ion carcinogenesis and human space exploration. Nat Rev 2008; 8:465–72.
51. Romero-Weaver AL, Lin L, Carabe-Fernandez A, Kennedy AR. Effects of solar particle event-like proton radiation and/or simulated microgravity on circulating mouse blood cells. Gravit Space Res 2014; 2:42–53.
52. Sanzari JK, Cengel KA, Wan XS, Rusek A, Kennedy AR. Acute hematological effects in mice exposed to the expected doses, dose-rates, and energies of solar particle event-like proton radiation. Life Sci Space Res 2014; 2:86–91.
53. Gridley DS, Rizvi A, Luo-Owen X, Makinde AY, Coutrakon GB, Koss P, et al. Variable hematopoietic responses to acute photons, protons and simulated solar particle event protons. In Vivo 2008; 22:159–69.
54. Shearer WT, Zhang S, Reuben JM, Lee BN, Butel JS. Effects of radiation and latent virus on immune responses in a space flight model. J Allergy Clin Immunol 2005; 115:1297–303.
55. Crucian BE, Cubbage ML, Sams CF. Altered cytokine production by specific human peripheral blood cell subsets immediately following space flight. J Interferon Cytokine Res 2000; 20:547–56.
56. Mehta SK, Stowe RP, Feiveson AH, Tyring SK, Pierson DL. Reactivation and shedding of cytomegalovirus in astronauts during spaceflight. The J Infect Dis 2000; 182:1761–4.
57. Lonart G, Parris B, Johnson AM, Miles S, Sanford LD, Singletary SJ, et al. Executive function in rats is impaired by low (20 cGy) doses of 1 GeV/u (56)Fe particles. Radiat Res 2012; 178:289–94.
58. Britten RA, Davis LK, Johnson AM, Keeney S, Siegel A, Sanford LD, et al. Low (20 cGy) doses of 1 GeV/u (56)Fe–particle radiation lead to a persistent reduction in the spatial learning ability of rats. Radiat Res 2012; 177:146–51.
59. Schultheis L, Ruff CB, Rastogi S, Bloomfield S, Hogan HA, Fedarko N, et al. Disuse bone loss in hindquarter suspended rats: partial weightbearing, exercise and ibandronate treatment as countermeasures. J Gravit Physiol 2000; 7:P13–4.
60. Kondo H, Yumoto K, Alwood JS, Mojarrab R, Wang A, Almeida EA, et al. Oxidative stress and gamma radiation-induced

cancellous bone loss with musculoskeletal disuse. J Appl Physiol 2010; 108:152–61.

61. Lloyd SA, Bandstra ER, Willey JS, Riffle SE, Tirado-Lee L, Nelson GA, et al. Effect of proton irradiation followed by hindlimb unloading on bone in mature mice: a model of long-duration spaceflight. Bone 2012; 51:756–64.

62. Yumoto K, Globus RK, Mojarrab R, Arakaki J, Wang A, Searby ND, et al. Short-term effects of whole-body exposure to (56)fe ions in combination with musculoskeletal disuse on bone cells. Radiat Res 2010; 173:494–504.

63. Alwood JS, Kumar A, Tran LH, Wang A, Limoli CL, Globus RK. Low-dose, ionizing radiation and age-related changes in skeletal microarchitecture. J Aging Res 2012; 2012:481983.

64. Alwood JS, Yumoto K, Mojarrab R, Limoli CL, Almeida EA, Searby ND, et al. Heavy ion irradiation and unloading effects on mouse lumbar vertebral microarchitecture, mechanical properties and tissue stresses. Bone 2010; 47:248–55.

65. Hu W, Pei H, Li H, Ding N, He J, Wang J, et al. Effects of shielding on the induction of 53BP1 foci and micronuclei after Fe ion exposures. J Radiat Res 2014; 55:10–6.

66. Loucas BD, Durante M, Bailey SM, Cornforth MN. Chromosome damage in human cells by gamma rays, alpha particles and heavy ions: track interactions in basic dose-response relationships. Radiat Res 2013; 179:9–20.

67. Datta K, Suman S, Kallakury BV, Fornace AJ, Jr. Exposure to heavy ion radiation induces persistent oxidative stress in mouse intestine. PLoS One 2012; 7:e42224.

68. Zhou Z, Ware JH, Kennedy AR. Carbon and iron ion radiation-induced cytotoxicity and transformation in vitro. Oncol Lett 2011; 2:915–18.

69. Lampidis TJ, Weichselbaum RR, Little JB. Letter: Gamma-irradiation of mammalian beating heart cells in vitro. Effects on cellular function. Int J Radiat Biol Relat Stud Phys Chem Med 1975; 28:99–102.

70. Petrovic D, Brown SM, Yatvin MB. Effects of adriamycin and irradiation on beating of rat heart muscle cells in culture. Int J Radiat Oncol Biol Phys 1977; 2:505–13.

71. Boerma M, van der Wees CG, Vrieling H, Svensson JP, Wondergem J, van der Laarse A, et al. Microarray analysis of gene expression profiles of cardiac myocytes and fibroblasts after mechanical stress, ionising or ultraviolet radiation. BMC Genomics 2005; 6:6.

72. Coleman MA, Sasi SP, Onufrak J, Natarajan M, Manickam K, Schwab J, et al. Low dose radiation affects cardiac physiology: gene networks and molecular signaling in cardiomyocytes. Am J Physiol Heart Circ Physiol 2015; 309:H1947–63.

73. Bisping E, Ikeda S, Kong SW, Tarnavski O, Bodyak N, McMullen JR, et al. Gata4 is required for maintenance of postnatal cardiac function and protection from pressure overload-induced heart failure. Proc Natl Acad of Sci USA 2006; 103:14471–6.

74. Wang X, Ren B, Liu S, Sentex E, Tappia PS, Dhalla NS. Characterization of cardiac hypertrophy and heart failure due to volume overload in the rat. J Appl Physiol 2003; 94:752–63.

75. Mihl C, Dassen WR, Kuipers H. Cardiac remodelling: concentric versus eccentric hypertrophy in strength and endurance athletes. Neth Heart J 2008; 16:129–33.

76. Lorell BH, Carabello BA. Left ventricular hypertrophy: pathogenesis, detection, and prognosis. Circulation 2000; 102:470–9.

77. Little WC. Heart failure with a normal left ventricular ejection fraction: diastolic heart failure. Trans Am Clin Climatol Assoc 2008; 119:93–9; discussion 99–102.

78. Oh JK, Hatle L, Tajik AJ, Little WC. Diastolic heart failure can be diagnosed by comprehensive two-dimensional and Doppler echocardiography. J Am Coll Cardiol 2006; 47:500–6.

79. Li C, Li J, Cai X, Sun H, Jiao J, Bai T, et al. Protein kinase D3 is a pivotal activator of pathological cardiac hypertrophy by selectively increasing the expression of hypertrophic transcription factors. J Biol Chem 2011; 286:40782–91.

80. Bushdid PB, Osinska H, Waclaw RR, Molkentin JD, Yutzey KE. NFATc3 and NFATc4 are required for cardiac development and mitochondrial function. Circ Res 2003; 92:1305–13.

81. Yang TT, Xiong Q, Enslen H, Davis RJ, Chow CW. Phosphorylation of NFATc4 by p38 mitogen-activated protein kinases. Mol Cell Biol 2002; 22:3892–904.

82. Tavernier B, Li JM, El-Omar MM, Lanone S, Yang ZK, Trayer IP, et al. Cardiac contractile impairment associated with increased phosphorylation of troponin I in endotoxemic rats. FASEB J 2001; 15:294–6.

83. Sakthivel S, Finley NL, Rosevear PR, Lorenz JN, Gulick J, Kim S, et al. In vivo and in vitro analysis of cardiac troponin I phosphorylation. J Biol Chem 2005; 280:703–14.

84. Grudzenski S, Raths A, Conrad S, Rube CE, Lobrich M. Inducible response required for repair of low-dose radiation damage in human fibroblasts. Proc Natl Acad of Sci U S A 2010; 107:14205–10.

85. Zhao Y, Zhong R, Sun L, Jia J, Ma S, Liu X. Ionizing radiation-induced adaptive response in fibroblasts under both monolayer and 3-dimensional conditions. PLoS One 2015; 10:e0121289.

86. Zhang F, Lin X, Yu L, Li W, Qian D, Cheng P, et al. Low-dose radiation prevents type 1 diabetes-induced cardiomyopathy via activation of AKT mediated anti-apoptotic and anti-oxidant effects. J Cell Mol Med 2016; 20:1352–66.

87. Hunter JJ, Chien KR. Signaling pathways for cardiac hypertrophy and failure. N Engl J Med 1999; 341:1276–83.

88. Hasenfuss G. Animal models of human cardiovascular disease, heart failure and hypertrophy. Cardiovasc Res 1998; 39:60–76.

89. Lloyd-Jones DM, Larson MG, Leip EP, Beiser A, D'Agostino RB, Kannel WB, et al. Lifetime risk for developing congestive heart failure: the Framingham Heart Study. Circulation 2002; 106:3068–72.

90. Vilahur G, Casani L, Pena E, Duran X, Juan-Babot O, Badimon L. Induction of RISK by HMG-CoA reductase inhibition affords cardioprotection after myocardial infarction. Atherosclerosis 2009; 206:95–101.

91. Zachary I, Gliki G. Signaling transduction mechanisms mediating biological actions of the vascular endothelial growth factor family. Cardiovasc Res 2001; 49:568–81.

92. Hausenloy DJ, Yellon DM. New directions for protecting the heart against ischaemia-reperfusion injury: targeting the Reperfusion Injury Salvage Kinase (RISK)-pathway. Cardiovasc Res 2004; 61:448–60.

93. Sun Y. Myocardial repair/remodelling following infarction: roles of local factors. Cardiovasc Res 2009; 81:482–90.

94. Kobayashi H, Minatoguchi S, Yasuda S, Bao N, Kawamura I, Iwasa M, et al. Post-infarct treatment with an erythropoietin-gelatin hydrogel drug delivery system for cardiac repair. Cardiovasc Res 2008; 79:611–20.

95. Fu X, Yang Y, Li X, Lai H, Huang Y, He L, et al. RGD peptide-conjugated selenium nanoparticles: antiangiogenesis by suppressing VEGF-VEGFR2-ERK/AKT pathway. Nanomedicine 2016; 12:1627–39.